Journal of Inflammation Research

Dovepress
Taylor & Francis Group

Open Access Full Text Article

ORIGINAL RESEARCH

Identification of Mitophagy-Related Genes and Analysis of Immune Infiltration in Atherosclerosis

Jiaqi Zhang, Xiting Wang, Xiahuan Chen, Meilin Liu

Department of Geriatrics, First Hospital, Peking University, Beijing, People's Republic of China

Correspondence: Meilin Liu, Email liumeilin@hotmail.com

Background: Atherosclerosis is a chronic inflammatory disease involving mitophagy and immune dysregulation. Currently, there is no integrated diagnostic model for autophagy immune genes in mitochondria. This study aimed to identify potential diagnostic markers through integrated bioinformatics and experimental validation.

Methods: Two atherosclerosis-related datasets (GSE43292 and GSE100927) were analyzed to identify differentially expressed mitophagy-related genes (MRGs), followed by enrichment analysis. Key genes were screened using LASSO, SVM-RFE, and random forest algorithms. A diagnostic nomogram was constructed and validated by ROC analysis. Immune infiltration was evaluated using CIBERSORT and ssGSEA. GSEA, GSVA, and unsupervised clustering were applied to explore biological pathways and molecular subtypes. qPCR validation was performed in ox-LDL-treated RAW264.7 and THP-1 cells.

Results: Thirteen upregulated and six downregulated MRGs were identified. Five hub genes (MNDA, CD163L1, NEXN, TC2N, SLC22A3) demonstrated strong diagnostic performance (AUC > 0.85) and were closely associated with immune cell infiltration; two molecular subtypes with distinct immune profiles were identified; qPCR validation confirmed the differential expression of these genes under inflammatory stimulation.

Conclusion: MNDA, CD163L1, NEXN, TC2N, and SLC22A3 may serve as diagnostic biomarkers for atherosclerosis. This five-gene model can stratify patient risk and guide personalized anti-inflammatory/autophagic therapy.

Keywords: atherosclerosis, mitophagy, immune infiltration, bioinformatics, cardiovascular disease

Introduction

Atherosclerosis is a complex and chronic inflammatory disease of the arteries, characterized by the formation of atherosclerotic plaques.[1] Its pathogenesis involves a combination of endothelial injury, lipid accumulation, and dysregulated immune responses that promote plaque development within the arterial wall. These pathological processes are exacerbated by well-established risk factors such as hypercholesterolemia, hypertension, diabetes, obesity, and smoking.[2] Despite significant advances in diagnostic and therapeutic strategies, atherosclerosis remains the leading cause of cardiovascular-related morbidity and mortality worldwide.[3] Therefore, identifying precise molecular markers and elucidating their roles in atherogenesis are essential steps toward improving the clinical diagnosis, risk stratification, and treatment of atherosclerotic disease.

Mitophagy, the selective autophagic degradation of damaged mitochondria, is vital for maintaining cellular homeostasis, particularly in vascular endothelial cells, smooth muscle cells, and macrophages—key players in atherosclerotic plaque development. Increasing evidence indicates that impaired mitophagy contributes to mitochondrial dysfunction and oxidative stress, thereby exacerbating vascular injury and disease progression.[4,5] Meanwhile, chronic inflammation—a hallmark of atherosclerosis—is driven by immune cell infiltration into the vascular wall,[6] where macrophages and T lymphocytes release pro-inflammatory cytokines (eg, interferon-γ) that promote plaque growth.[7] Recent studies suggest that mitophagy and immune cell infiltration are interconnected processes in various diseases,[8] and this crosstalk may play a pivotal role in determining the initiation, progression, and stability of atherosclerotic plaques. For instance, mitophagy helps reduce inflammation by clearing dysfunctional mitochondria, which would otherwise serve as danger signals to activate immune pathways. It also modulates immune responses by promoting M2-type macrophage polarization and

Received: 11 June 2025
Accepted: 17 September 2025
Published: 3 October 2025

influencing T-cell activation and differentiation.[9] However, most studies to date have focused on mitophagy or immune mechanisms independently, leaving the interplay between these processes in the context of atherosclerosis largely unexplored. This gap highlights the need for an integrative approach that examines mitophagy and immune regulation concurrently to uncover new mechanistic insights and identify novel therapeutic targets.

In this study, we conducted an integrated bioinformatics analysis using two publicly available human gene expression datasets (GSE43292 and GSE100927)[10,11] to identify differentially expressed MRGs in atherosclerotic tissues. We further explored the relationship between these MRGs and immune cell infiltration. To validate our findings, we examined the expression of candidate genes in ox-LDL–stimulated macrophage models using quantitative PCR (qPCR). Collectively, our results provide new evidence that genes involved in mitophagy and immunity contribute to the pathogenesis of atherosclerosis and may serve as promising diagnostic biomarkers and therapeutic targets.

Materials and Methods

Data Acquisition

Atherosclerosis-related microarray datasets GSE43292[10] and GSE100927[11] were obtained from the NCBI Gene Expression Omnibus (GEO) database using the GEOquery package (version 2.76.0).[12] GSE43292 (GPL6244 platform) contained 64 samples (32 atherosclerotic lesions and 32 non-atherosclerotic controls), and GSE100927 (GPL17077 platform) comprised 104 samples (69 atherosclerotic and 35 controls). A total of 2,414 MRGs were identified from GeneCards by searching the term "mitophagy", and these are listed in Table S1.[13]

Differential Analysis

The two GEO datasets were merged, and batch effects were corrected using the ComBat algorithm implemented in the sva package (version 3.56.0).[14] We verified successful batch effect removal by comparing sample expression distributions on boxplots before and after ComBat adjustment, which showed aligned medians across batches. Quantile normalization was applied as needed in conjunction with ComBat, following best-practice recommendations. After batch correction, differential expression analysis was performed using the limma package (version 3.64.1).[15] Genes with $|\log_2 FC| > 1$ and adjusted $P < 0.05$ were considered differentially expressed genes (DEGs). Results were visualized with pheatmap (version 1.0.13) heatmaps and ggplot2 (version 3.5.2) volcano plots.

Enrichment Analysis

Gene Ontology (GO)[16] and Kyoto Encyclopedia of Genes and Genomes (KEGG)[17] pathway enrichment analyses were performed to investigate the biological functions of the identified MRGs. We utilized the WebGestalt toolkit[18] for GO and KEGG analyses, with statistical significance defined as $P < 0.05$.

Selection of Feature Genes

Key diagnostic genes (hub genes) were identified using multiple machine-learning approaches. Least absolute shrinkage and selection operator (LASSO) regression, support vector machine-recursive feature elimination (SVM-RFE), and random forest algorithms were applied to the DEGs. These methods were implemented using the glmnet package (version 4.1–10) for LASSO, the e1071 package for SVM-RFE,[19] and the randomForest package (version 4.7–1.2) for random forest modeling.[20]

The top-performing hub genes were further evaluated with a nomogram for diagnostic prediction. A nomogram was constructed using the rms package (version 8.0–0)[21] to illustrate the contribution of each hub gene to atherosclerosis risk. Calibration curves were plotted to assess the agreement between predicted risk and actual outcomes. The diagnostic performance was quantified by the area under the receiver operating characteristic curve (AUC), calculated using the pROC package (version 1.18.5).[22]

Gene Set Enrichment and Variation Analysis

To explore pathway-level differences, gene set enrichment analysis (GSEA) and gene set variation analysis (GSVA) were performed. Samples were stratified into high-risk and low-risk groups based on the median risk score derived from the diagnostic model. GSEA was conducted using the clusterProfiler package (version 4.16.0) with the c2.all.v7.2 curated gene set from the MSigDB database as the reference, and a significance threshold of $P < 0.05$ was applied.[23,24] In parallel, GSVA (version 2.2.0) was used to estimate the variation in pathway activity across individual atherosclerotic samples based on their gene expression matrices.[25] Differentially enriched pathways between the high- and low-risk groups were identified using the limma package, with thresholds set at $|\log_2 FC| > 1$ and adjusted $P < 0.05$.[15]

Network Construction

Protein-protein interaction (PPI) networks were constructed using STRING (Search Tool for the Retrieval of Interacting Genes/Proteins)[26] to explore interactions among hub genes. Additionally, mRNA–miRNA and mRNA–RBP regulatory networks were obtained from starBase.[27] Transcription factor (TF) binding predictions were conducted using the PROMO database,[28] resulting in comprehensive mRNA–miRNA, mRNA–RBP, and mRNA–TF interaction networks.

Immune Analysis

Immune cell infiltration was evaluated using the CIBERSORT algorithm[29] based on expression profiles of 22 immune cell types. Additionally, single-sample gene set enrichment analysis (ssGSEA)[30] was used to quantify 28 types of immune cells and immune response activities in individual samples. Visualizations of immune cell distributions were created using ggplot2. Correlations between hub gene expression and immune cell abundance were further analyzed, and differences in immune infiltration among atherosclerotic subtypes were explored.

Clustering Analysis

Unsupervised consensus clustering was performed using the ConsensusClusterPlus package (version 1.72.0)[31] to classify atherosclerotic samples into molecular subtypes.

Cell Culture and Treatment

RAW264.7 (mouse macrophage cell line) and THP-1 (human monocyte cell line) were purchased from Procell (Wuhan, China). RAW264.7 cells were cultured in DMEM supplemented with 10% fetal bovine serum (FBS), and THP-1 cells were cultured in RPMI1640 with 10% FBS. Both cell lines were maintained at 37°C in a humidified atmosphere with 5% CO_2. To induce macrophage differentiation, THP-1 cells were treated with 100 ng/mL phorbol 12-myristate 13-acetate (PMA, Sigma) for 48 hours.

To simulate the pro-inflammatory environment of atherosclerotic lesions in vitro, cells were divided into control and experimental groups. Experimental cells were treated with oxidized low-density lipoprotein (ox-LDL, 50 μg/mL; Yiyuan Biotech, Guangzhou, China) for 24 h. This ox-LDL stimulation induces macrophage foam-cell formation and mimics atherosclerotic inflammatory conditions, as established in previous studies.[32,33] All cell experiments were performed in triplicate independent runs (n = 3) to ensure reproducibility.

RNA Extraction and cDNA Synthesis

Total RNA was extracted from treated cells using TRIzol reagent (Invitrogen, USA) according to the manufacturer's protocol. RNA purity and concentration were assessed using NanoDrop spectrophotometer (Thermo Scientific). Reverse transcription was conducted using PrimeScript™ RT Reagent Kit (TaKaRa, Japan) following manufacturer's instructions, obtaining cDNA templates for subsequent qPCR analysis.

Quantitative Real-Time PCR (qPCR)

qPCR was performed with SYBR Green Master Mix (TaKaRa) on an ABI 7500 Real-Time PCR System. Cycling conditions were: 95°C for 30s, followed by 40 cycles of 95°C for 5 s and 60°C for 30s. Relative gene expression was

calculated by the $2^{-\Delta\Delta Ct}$ method using β-actin (mouse) or GAPDH (human) as internal controls. Primer sequences are listed below:

Mouse primers: Mnda (forward 5′-GACAACCAAGAGCAATACACCA-3′, reverse 5′-ATCAGTTTGCCCAATCCAGAAT-3′), Cd163l1 (forward 5′-CTGGCCTCTGAGTTTAGGGTC-3′, reverse 5′-CCCTTGGTGTCGAACCAGC-3′), Nexn (forward 5′-ATGAATGACGTTTCGCAAAAGG-3′, reverse 5′-GCTAATTCGCGCTGTATTTTCC-3′), Tc2n (forward 5′-CCATTGGTATCCCTCCATTGAC-3′, reverse 5′-GGGCACCACAAATTGTACTTCTT-3′), Slc22a3 (forward 5′-CAGCCCGACTACTATTGGTGT-3′, reverse 5′-TGAGCTGGTATTAGTGGCTTCC-3′); β-Actin (forward 5′-TCCGGCACTACCGAGTTATC-3′, reverse 5′-GATCCGGTGTAGCAGATCGC-3′).

Human primers: MNDA (forward 5′-GTTTACTCCGAATCAGGAAACCC-3′, reverse 5′-TAAATGGCGCTGTTGCTTTCA-3′), CD163L1 (forward 5′-GCTGTGGTAACTTGCATCCTG-3′, reverse 5′-GCAGTAGTGTTCCACCCATCA-3′), NEXN (forward 5′-ACTGTGAAGGGTAGATTTGCTG-3′, reverse 5′-TTCTGCGTTTTCGTTCCTCCT-3′), TC2N (forward 5′-TGGCTGTACTGAGGATTATTTGC-3′, reverse 5′-TGTGAAGGAGTTTCTTGTGTCC-3′), SLC22A3 (forward 5′-CTTCCGCTTCCTGCAAGGT-3′, reverse 5′-AAGTAGGCAATTCCAGGGAGA-3′); GAPDH (forward 5′-TGCACCACCAACTGCTTAGC-3′, reverse 5′-GGCATGGACTGTGGTCATGAG-3′).

Statistical Analysis

All statistical analyses were performed in R (version 3.6.3). Package versions used throughout the analysis are specified above to ensure reproducibility and statistical rigor.

Results

Overview of DEGs in Atherosclerosis

The workflow of this study is illustrated in Figure 1. The datasets used in this study are summarized in Table 1. Figure 2A and B show the uncorrected and corrected boxplots of datasets GSE43292 and GSE100927, respectively. Differential expression analysis between the Atherosclerotic and Control groups in the merged datasets identified 182 DEGs meeting the criteria $|\log_2 FC| > 1$ and P.adj < 0.05, comprising 136 upregulated and 46 downregulated genes (Figure 2C). The most significantly upregulated genes were MMP9, IBSP, ACP5, MMP7, and MMP12, whereas the most significantly downregulated genes were PI16, CASQ2, DES, PLA2G2A, and MYOC (Figure 2D).

Identification of MRGs

A cross-analysis with 2,414 MRGs yielded 13 upregulated (HMOX1, FABP5, APOE, FBP1, C15orf48, MS4A4A, ITGAX, VAMP8, CD163L1, IL1B, CA2, CTSD, and MNDA) and six downregulated (SLC22A3, NEXN, MYOM1, FLNC, TC2N, and CASQ2) MRGs (Figure 3A). The chromosomal locations of these 19 genes are shown in Figure 3B. Their expression patterns are displayed in the heatmap (Figure 3C), volcano plot (Figure 3D), and boxplots (Figure 3E). Across all three visualization approaches, HMOX1, FABP5, APOE, FBP1, C15orf48, MS4A4A, ITGAX, VAMP8, CD163L1, IL1B, CA2, CTSD, and MNDA were markedly upregulated in the Atherosclerotic group, whereas SLC22A3, NEXN, MYOM1, FLNC, TC2N, and CASQ2 were significantly downregulated. Correlations among the 19 genes are presented in Figure 4A. ROC curves for MNDA, CD163L1, TC2N, and SLC22A3 showed AUC values above 0.85 in atherosclerotic tissue (Figure 4B–D).

Enrichment Analyses of MRGs

In this study, functional enrichment analyses were performed using the GO and KEGG databases to understand the potential functions and pathways of MRGs in the development of atherosclerosis (Tables 2, 3 and Figure 5). GO enrichment analysis was performed to determine the biological characteristics of the DEGs, and the results were divided into three functional categories: biological processes (BP), cell components (CC), and molecular functions (MF). The MRGs were mainly associated with biological processes, such as response to stimulus, localization, biological regulation, cell communication, cellular component organization, multicellular organismal processes, developmental processes, and

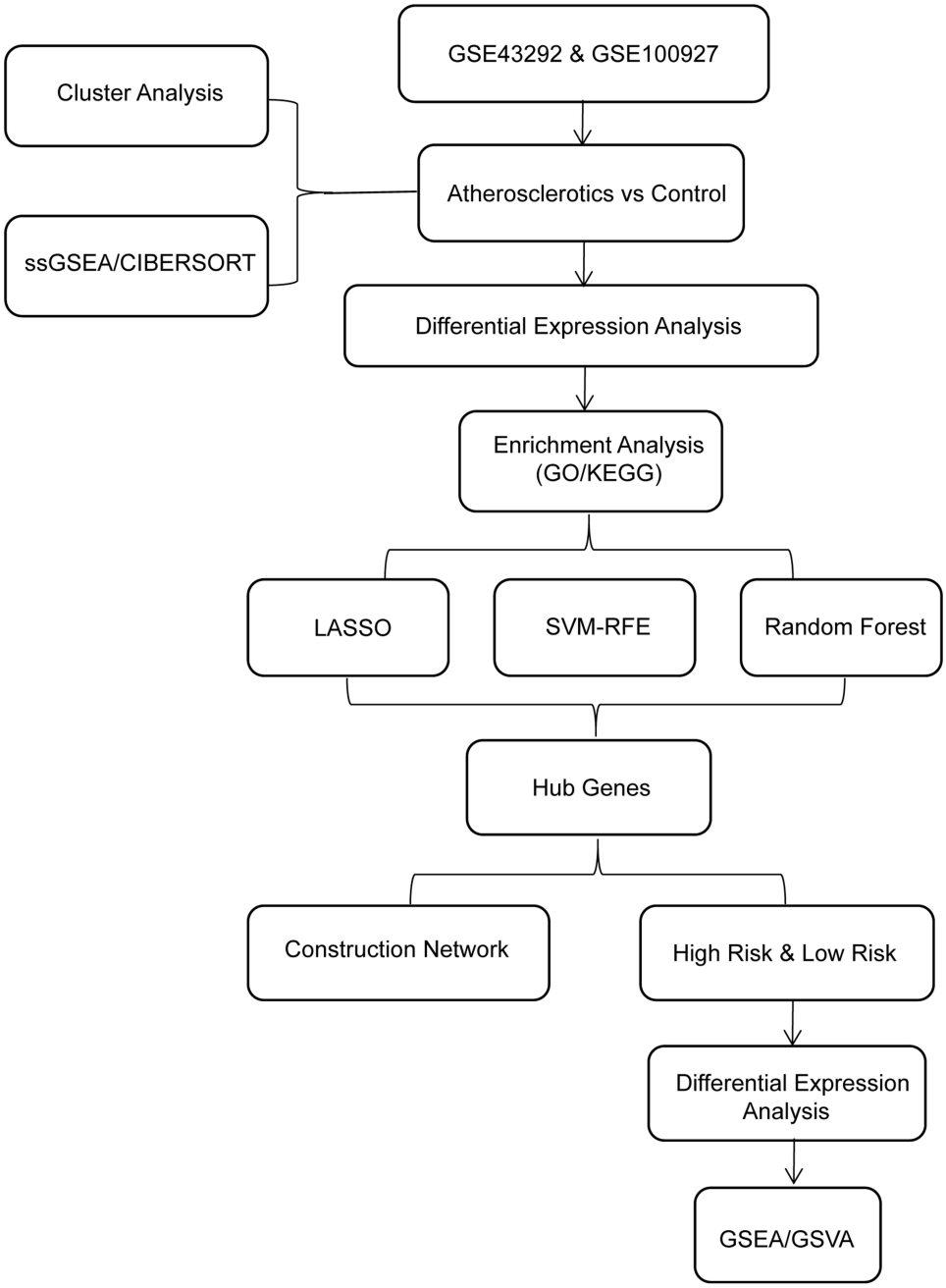

Figure 1 Research design flowchart.
Abbreviations: GO, Gene Ontology; KEGG, Kyoto Encyclopedia of Genes and Genomes; LASSO, Least absolute shrinkage and selection operator; SVM-RFE, support vector machine-recursive feature elimination; GSEA, Gene set enrichment analysis; GSVA, Gene set variation analysis; ssGSEA, single-sample gene set enrichment analysis; CIBERSORT, cell-type identification by estimating relative subsets of RNA transcripts.

metabolic processes (Figure 5A–C and Table 2). KEGG analysis identified enrichment in pathways, such as the pentose phosphate pathway, antifolate resistance, autophagy, fluid shear stress, and atherosclerosis (Figure 5D and Table 3, $P < 0.05$). The pathway maps are shown in Figure S1.

Table 1 Dataset Information

GEO Data Set	Platform	Control	Atherosclerotic
GSE43292	GPL6244	32	32
GSE100927	GPL17077	35	69

https://doi.org/10.2147/JIR.S544597

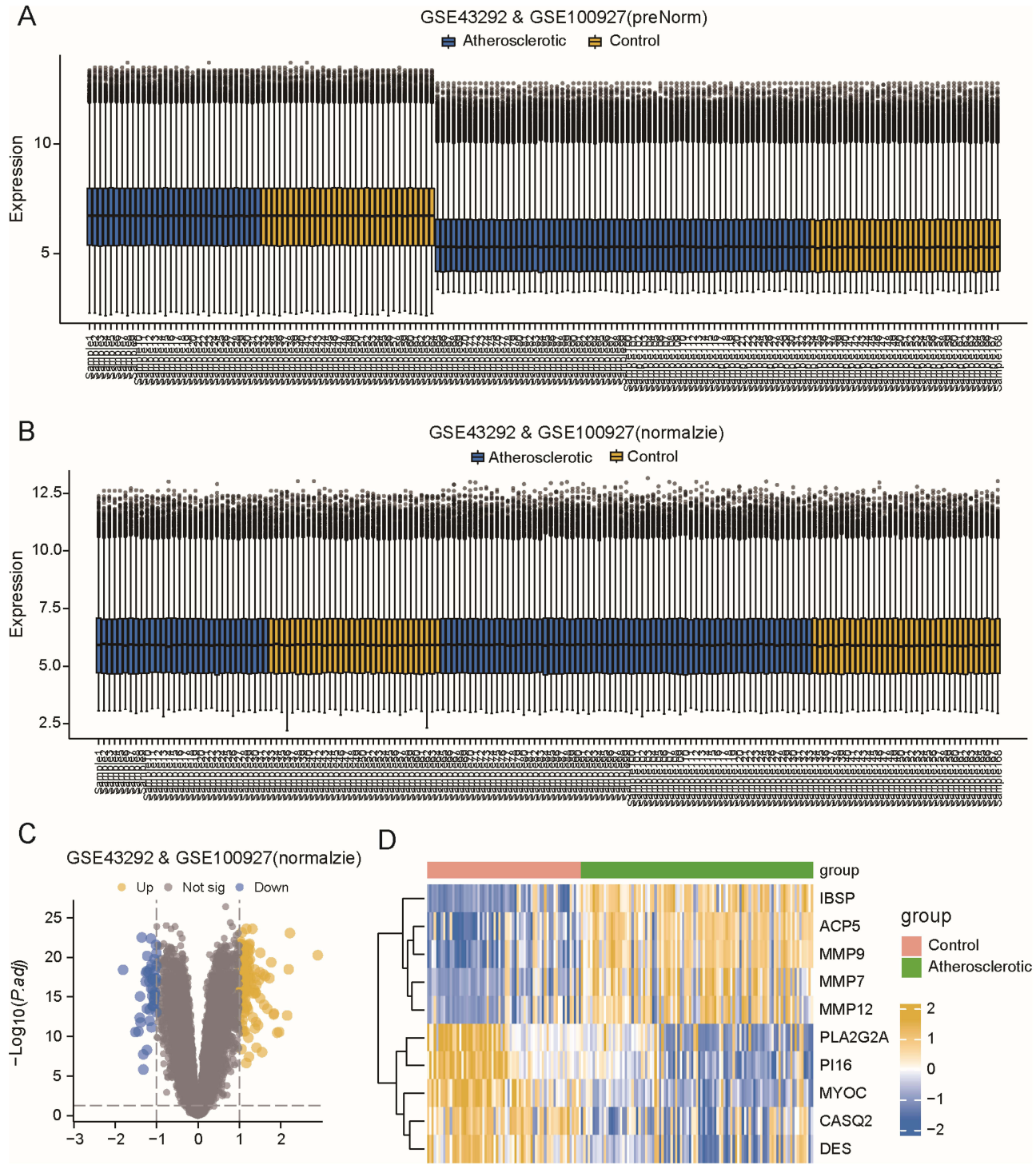

Figure 2 Comparative analysis of Atherosclerotic and Control samples. (**A**) Pre-normalization boxplot for datasets GSE43292 and GSE100927. (**B**) Post-normalization boxplot for datasets GSE43292 and GSE100927. (**C**) Volcano plot highlighting the differentially expressed genes (DEGs) between the Atherosclerotic and Control groups. (**D**) Heatmap representing the top five upregulated and downregulated DEGs in the Atherosclerotic and Control groups.

Hub Gene Selection by Machine Learning

LASSO logistic regression analysis (Figure S2A) identified 18 genes from 19 MRGs (Figure S2B). The SVM-RFE algorithm further refined this to 16 genes with an accuracy of 0.923 (Figure S2C) and an error rate of 0.0774 (Figure S2D). The

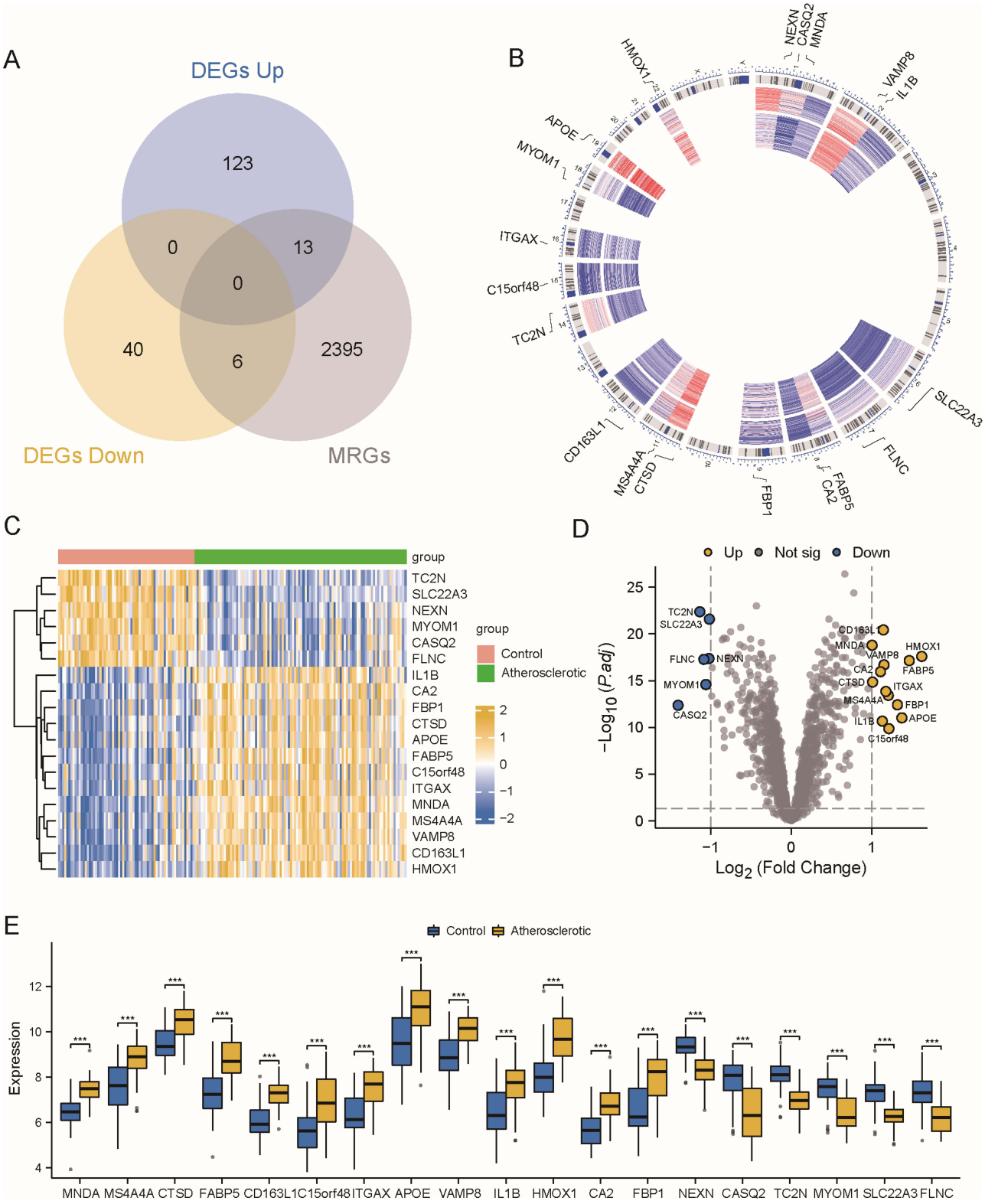

Figure 3 Analysis of mitophagy-related gene expression in Atherosclerotic and Control samples. (**A**) Venn diagram illustrating the overlap between differentially expressed genes (DEGs) and mitophagy-related genes (MRGs). (**B**) Chromosomal localization of differentially expressed mitophagy genes. (**C**) Heatmap displaying the differential expression of mitophagy genes in the Atherosclerotic and Control groups (yellow = high expression and blue = low expression). (**D**) Volcano plot showing differential expression analysis of mitophagy genes between the Atherosclerotic and Control groups. (**E**) Expression profile of differentially expressed mitophagy genes in the Atherosclerotic and Control groups.

Note: (***$P < 0.001$).

https://doi.org/10.2147/JIR.S544597

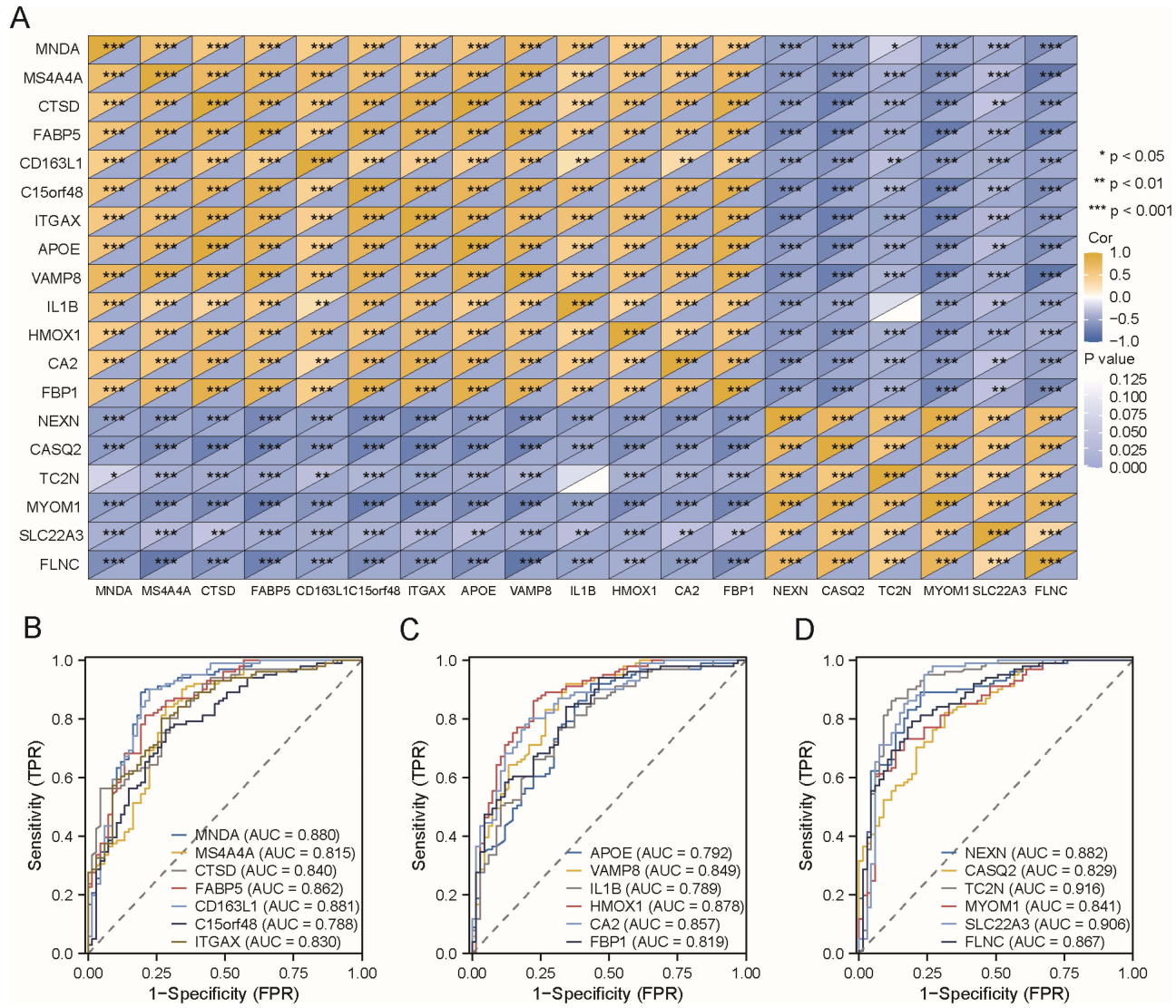

Figure 4 Correlation and diagnostic analysis of differentially expressed mitophagy genes in the combined dataset. (**A**) Heatmap illustrating the correlations between differentially expressed mitophagy genes in Atherosclerotic samples, with yellow indicating positive correlation and blue indicating negative correlation. (**B-D**) Diagnostic receiver operating characteristic (ROC) curves for selected differentially expressed mitophagy genes in the Atherosclerotic and Control groups: (**B**) MNDA, MS4A4A, CTSD, FABP5, CD163L1, C15orf48, ITGAX (**C**) APOE, VAMP8, IL1B, HMOX1, CA2, FBP1 (**D**) NEXN, CASQ2, TC2N, MYOM1, SLC22A3, FLNC.
Note: (*P < 0.05; **P < 0.01; ***P < 0.001).

relationship between the number of decision trees and errors in RF model construction is shown in Figure S2E, including the top six important MRGs (SLC22A3, TC2N, CD163L1, MNDA, HMOX1, and NEXN) (Figure S2F).

The intersection of the three algorithms yielded five diagnosis-related hub genes: MNDA, CD163L1, NEXN, TC2N, and SLC22A3 (Figure 6A). Individual gene AUCs showed high diagnostic efficiency (AUC > 0.85), indicating high diagnostic value (Figure 6B). A line graph constructed using the hub genes is shown in Figure 6C. A calibration plot illustrated good agreement between the actual and predicted probabilities of atherosclerotic diagnosis (Figure 6D), demonstrating that the model possessed robust diagnostic efficacy.

GSEA and GSVA Analyses

Patients with atherosclerosis were stratified into high- and low-risk groups based on the median risk score from the hub gene model. Differential expression analysis between these groups identified 26 DEGs ($|\log_2 FC| > 1$, P.adj < 0.05), including 10 upregulated and 16 downregulated genes in the high-risk group (Figure 7A). The top five upregulated and

Table 2 Gene Ontology Enrichment Analysis

	Gene Set	Description	Size
BP	GO:0050896	Response to stimulus	15
BP	GO:0051179	Localization	15
BP	GO:0065007	Biological regulation	13
BP	GO:0007154	Cell communication	11
BP	GO:0016043	Cellular component organization	10
BP	GO:0032501	Multicellular organismal process	10
BP	GO:0032502	Developmental process	10
BP	GO:0008152	Metabolic process	9
BP	GO:0051704	Multi-organism process	5
BP	GO:0008283	Cell proliferation	4
BP	GO:0040007	Growth	2
BP	GO:0000003	Reproduction	1
CC	GO:0016020	Membrane	14
CC	GO:0005615	Extracellular space	9
CC	GO:0012505	Endomembrane system	9
CC	GO:0031982	Vesicle	9
CC	GO:0005634	Nucleus	7
CC	GO:0005829	Cytosol	7
CC	GO:0031974	Membrane-enclosed lumen	6
CC	GO:0032991	Protein-containing complex	6
CC	GO:0005773	Vacuole	5
CC	GO:0005783	Endoplasmic reticulum	3
CC	GO:0042995	Cell projection	3
CC	GO:0005856	Cytoskeleton	3
CC	GO:0005768	Endosome	2
CC	GO:0031012	Extracellular matrix	2
CC	GO:0005794	Golgi apparatus	1
CC	GO:0005739	Mitochondrion	1
CC	GO:0031975	Envelope	1
MF	GO:0005515	Protein binding	16
MF	GO:0043167	Ion binding	7
MF	GO:0016787	Hydrolase activity	4
MF	GO:0005198	Structural molecule activity	3
MF	GO:0005215	Transporter activity	3
MF	GO:0008289	Lipid binding	2
MF	GO:0016209	Antioxidant activity	1
MF	GO:0030234	Enzyme regulator activity	1
MF	GO:0000166	Nucleotide binding	1
MF	GO:0030246	Carbohydrate binding	1
MF	GO:0009055	Electron transfer activity	1
MF	GO:0060089	Molecular transducer activity	1
MF	GO:0003676	Nucleic acid binding	1

downregulated genes are displayed in Figure 7B. GSEA identified pathways enriched in the high-risk group, including the WP IL-18 signaling pathway, KEGG chemokine signaling pathway, Alcala apoptosis, and WP B cell receptor signaling pathway (Figure 7C and Table 4). GSVA revealed that the GO positive regulation of cardiac vascular smooth muscle cell differentiation pathway was enriched in the low-risk group (Figure 7D and Table 5).

https://doi.org/10.2147/JIR.S544597

Table 3 Kyoto Encyclopedia of Genes and Genomes Enrichment Analysis

Gene Set	Description	Size	P value
hsa00030	Pentose phosphate pathway	30	0.047134
hsa00910	Nitrogen metabolism	17	0.026963
hsa01523	Antifolate resistance	30	0.047134
hsa04140	Autophagy	127	0.01679
hsa04964	Proximal tubule bicarbonate reclamation	23	0.03632
hsa04966	Collecting duct acid secretion	27	0.042513
hsa05010	Alzheimer disease	170	0.029031
hsa05132	Salmonella infection	83	0.0074215
hsa05152	Tuberculosis	178	0.0024358
hsa05418	Fluid shear stress and atherosclerosis	136	0.019113

Network Construction

A PPI network of the hub genes was constructed using the STRING database (Figure 8A). Specifically, MNDA interacted with TYROBP and NCF2, whereas NEXN interacted with CTNNB1, CTTN, DBN1, and GRN, and CTNNB1 engaged with SLC22A3. Additionally, mRNA-miRNA interaction networks were derived from starBase (Figure 8B and Table S2). This network included interactions, such as CD163L1 with hsa-miR-146a-5p and hsa-miR-589-5p, and MNDA with hsa-miR-541-3p. The mRNA-RBP interaction network, predicted using the same database, is shown in Figure 8C. RPBs associated with CD163L1 included ACIN1, ADAR, BCCIP, BUD13, CNBP, whereas those associated with MNDA consisted of ELAVL1, FUS, HNRNPL, MSI2, TAF15, TROVE2. The predicted mRNA-TF network was based on the PROMO database (Figure 8D). TFs, such as Pax-5, p53, AP-2alphaA, NFI/CTF, TFII-I, GR-alpha, RXR-alpha, STAT4, ER-alpha, GCF, and Sp1, interacted with SLC22A3.

Immune Cell Infiltration Analysis

Using CIBERSORT, the abundance of 22 immune cell types was assessed in the Control, high-, and low-risk Atherosclerotic samples (Figure 9A). Notably, M0 macrophages were more abundant in Atherosclerotic samples than those in Control samples, and were also elevated in the high-risk versus low-risk Atherosclerotic groups. The heatmap in Figure 9B illustrates the correlations between hub genes and the infiltration levels of these immune cells in Atherosclerotic samples. Specifically, MNDA (Figure 9C) and CD163L1 (Figure 9D) were negatively correlated with plasma cells ($R < 0$, $P < 0.05$), whereas NEXN (Figure 9E) and CD163L1 (Figure 9F) were positively correlated with M2 macrophages and memory B cells, respectively ($R > 0$, $P < 0.05$).

ssGSEA was further used to assess the abundance of 28 immune cell types in the Control, high-, and low-risk Atherosclerotic groups (Figure 10A). There was an increased abundance of several immune cells in the Atherosclerotic samples compared to that in the Control, as well as in high-risk versus low-risk Atherosclerotic samples. The heatmap in Figure 10B shows significant positive correlations between MNDA, CD163L1, and several immune cells ($R > 0$, $P < 0.05$) and significant negative correlations between NEXN, TC2N, SLC22A3, and various immune cells ($R < 0$, $P < 0.05$).

Consensus Clustering of Atherosclerosis

Unsupervised consensus clustering was employed to identify the molecular subtypes of atherosclerotic disease based on the expression profile data (Figure 11A). The expression profiles of the hub genes, differentiated into two unique atherosclerotic subtypes, are shown in Figure 11B. MNDA and CD163L1 were markedly overexpressed in cluster B, whereas TC2N and SLC22A3 were significantly underexpressed in the same cluster. Additionally, immune cell infiltration analysis across different clusters suggested variations in the presence of specific immune cells, such as M0 macrophages, among the different subtypes (Figure 11C).

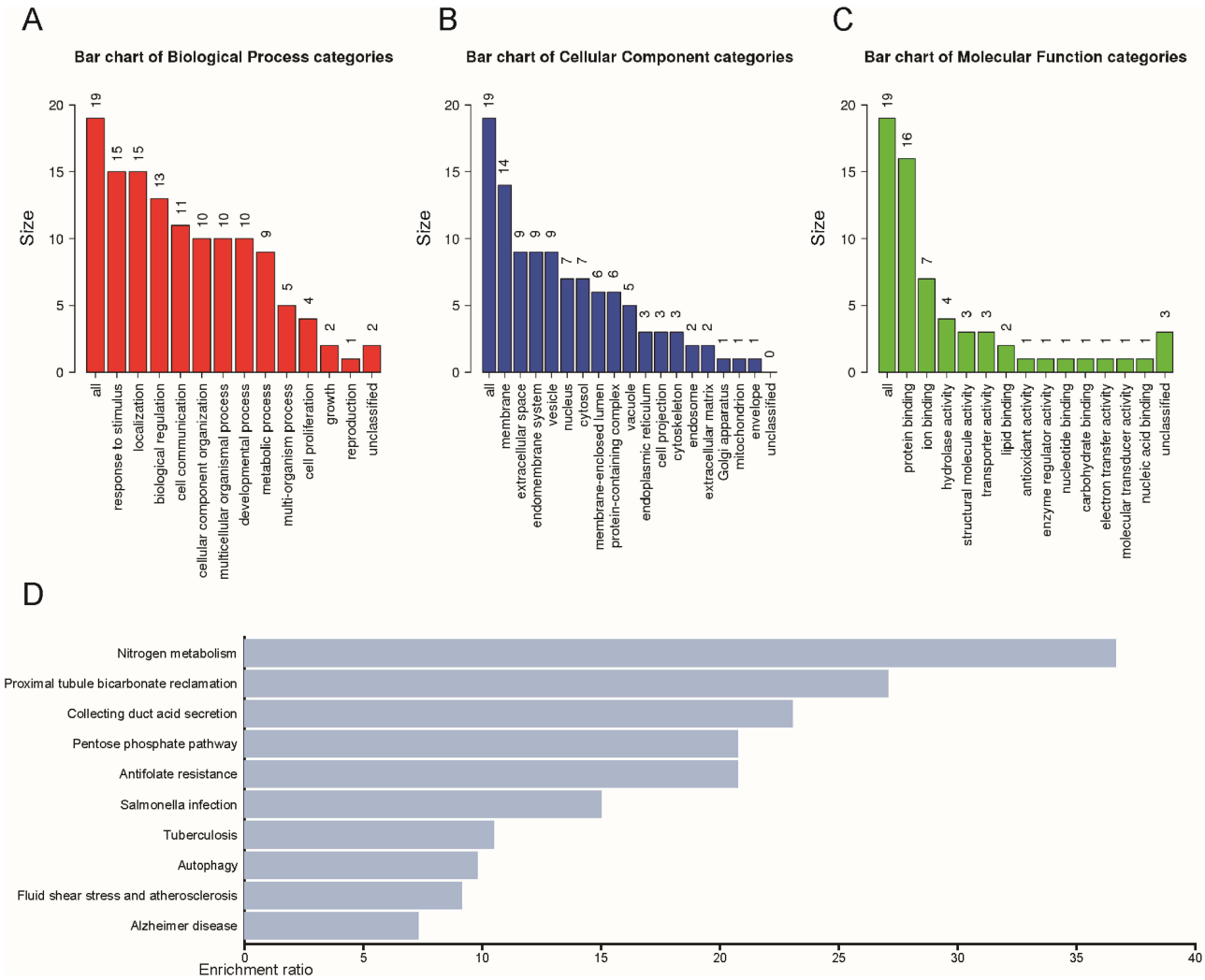

Figure 5 GO and KEGG enrichment analysis of differentially expressed mitophagy genes in the combined dataset. (**A-C**) Enrichment analysis of differentially expressed mitophagy genes in the Atherosclerotic and Control groups, targeting (**A**) Biological Process, (**B**) Cellular Component, (**C**) Molecular Function. (**D**) Kyoto Encyclopedia of Genes and Genomes pathways.
Abbreviations: GO, Gene Ontology; KEGG, Kyoto Encyclopedia of Genes and Genomes.

qPCR Validation of Candidate Genes

To validate the expression of candidate MRGs, qPCR was performed in RAW264.7 and THP-1 cells treated with ox-LDL to simulate an atherosclerosis-related inflammatory environment. In RAW264.7 cells, the expression of Mnda and Cd163l1 was significantly increased, while Nexn, Tc2n, and Slc22a3 were downregulated (Figure 12A). In THP-1 cells, MNDA expression was significantly elevated; CD163L1 showed no significant change. NEXN and SLC22A3 were downregulated, whereas TC2N expression remained unchanged (Figure 12B).

Discussion

Our findings underscore the critical interplay between impaired mitophagy and immune dysregulation in atherosclerosis. In this study, we identified 19 differentially expressed MRGs in atherosclerotic lesions through integrated bioinformatic analysis. These genes were enriched in metabolism- and inflammation-related pathways – notably the pentose phosphate pathway, autophagy, and the "fluid shear stress and atherosclerosis" pathway – suggesting that disturbances in mitochondrial quality control can influence key atherogenic processes. For example, inhibiting the pentose phosphate pathway is known to alter macrophage metabolism and phenotype, thereby attenuating inflammatory responses and slowing plaque

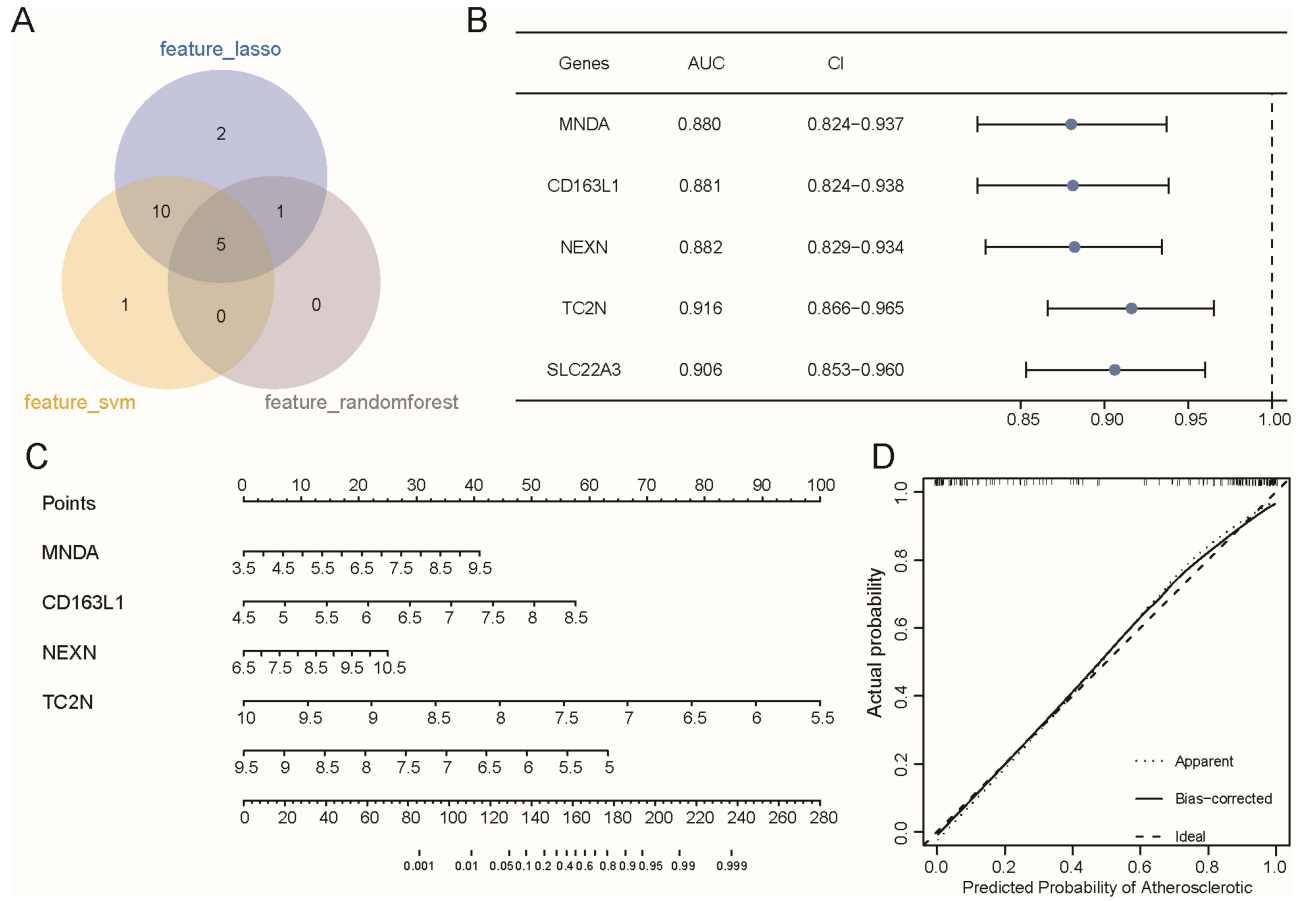

Figure 6 Analysis of hub genes derived from the combined dataset. (**A**) Venn diagram depicting the feature genes selected using the three distinct algorithms. (**B**) Forest plot illustrating the AUC for the identified hub genes. (**C**) Line plots constructed from the selected hub genes. (**D**) Calibration plot derived from the line plot model. Area Under the Curve, AUC.

progression.[34] Similarly, aberrant mechanosensory signaling (as indicated by enrichment of the shear stress pathway) can exacerbate endothelial injury and inflammation via mechanisms such as bone morphogenetic protein-9/ALK1-mediated SMAD activation.[35,36] Thus, the enrichment analysis supports the concept that mitophagy-associated genes are functionally intertwined with the pathways driving atherosclerotic plaque development.

Using three machine-learning algorithms (LASSO, SVM-RFE, and random forest), we pinpointed five hub genes with high diagnostic value for atherosclerosis: MNDA, CD163L1, NEXN, TC2N, and SLC22A3. Each of these genes plays a distinct role in cellular function and immune regulation, shedding light on their potential contributions to atherogenesis.

MNDA (myeloid cell nuclear differentiation antigen) is expressed specifically in the nuclei of granulocyte-monocyte lineage cells and is involved in inflammation and apoptosis.[37,38] It can regulate interferon signaling in monocytes via interferon regulatory factor 7 (IRF7),[39] and it has been linked to autoimmune diseases such as rheumatoid arthritis.[40] In our analysis, MNDA was significantly up-regulated in atherosclerotic tissues and positively correlated with immune cell infiltration, suggesting that MNDA may promote pro-inflammatory activation within plaques.CD163L1 (CD163-like 1) is a membrane receptor mainly found on monocytes and macrophages,[41] closely related to the scavenger receptor CD163. CD163L1 and CD163 are known for their roles in immune regulation and the resolution of inflammation. High levels of CD163-positive macrophages have been observed in metabolic and fibrotic diseases.[42,43] Moreover, modulating these macrophages can influence immune responses; for example, interferon-γ (IFN-γ) enhances CAR T-cell efficacy by affecting $CD163^{+}$ M2 macrophages.[44] The elevated expression of CD163L1 in atherosclerotic lesions in our study suggests a potential involvement in macrophage-driven inflammation or in feedback mechanisms that limit excessive inflammation within plaques.NEXN (Nexilin) is a cytoskeletal protein critical for cardiovascular cell integrity due to its

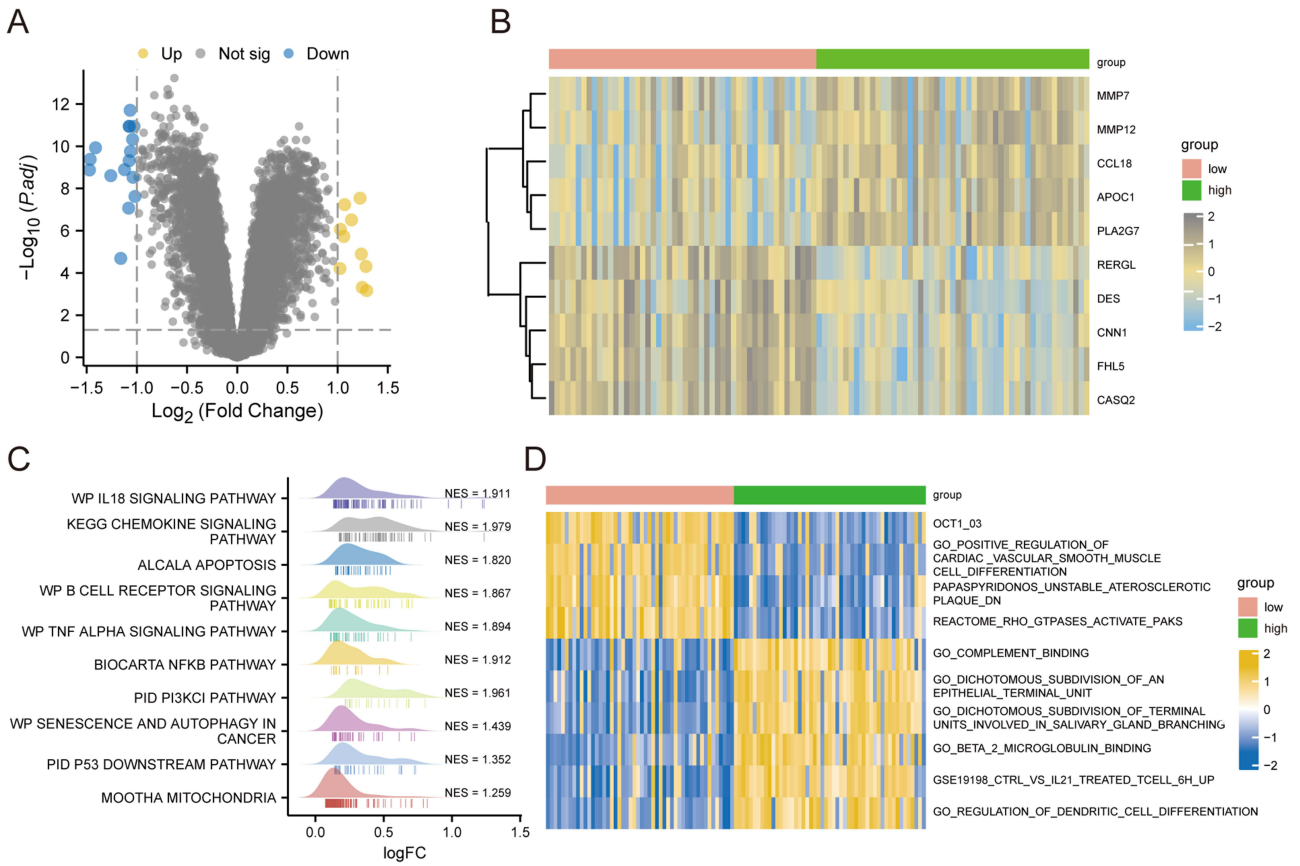

Figure 7 Differential analysis between high- and low-risk groups in patients with atherosclerosis from the combined dataset. (**A**) Volcano plot illustrating differential gene expression between high- and low-risk groups; yellow indicates upregulated genes, and blue indicates downregulated genes. (**B**) Heatmap of the top five upregulated and downregulated differential genes, with yellow representing upregulated genes and blue representing downregulated genes. (**C**) Mountain plot of GSEA based on high- and low-risk groups. (**D**) Heatmap of GSVA based on high- and low-risk groups, where blue signifies $log_2FC < 0$ and yellow signifies $log_2FC > 0$.
Abbreviations: GSEA, Gene set enrichment analysis; GSVA, Gene set variation analysis.

F-actin binding and role in muscle development.[45] Notably, NEXN has an anti-inflammatory effect in the vasculature. For example, the long non-coding RNA NEXN-AS1 increases NEXN expression, which in turn inhibits Toll-like receptor 4 (TLR4)/NF-κB signaling and reduces adhesion molecule and cytokine levels in endothelial cells; consequently, NEXN helps block monocyte adhesion and mitigates atherosclerosis.[46] Consistent with this protective role, we found NEXN to be significantly down-regulated in atherosclerotic tissues—a change that could remove an important brake on inflammatory cell recruitment and plaque formation.TC2N (tandem C2 domains, nuclear) encodes a nuclear

Table 4 Gene Set Enrichment Analysis

Description	Setsize	NES	P value
WP_IL18_SIGNALING_PATHWAY	254	1.910765637	0.001597444
KEGG_CHEMOKINE_SIGNALING_PATHWAY	172	1.979137305	0.001650165
ALCALA_APOPTOSIS	80	1.82034905	0.001712329
WP_B_CELL_RECEPTOR_SIGNALING_PATHWAY	94	1.866728646	0.001733102
WP_TNF_ALPHA_SIGNALING_PATHWAY	90	1.893610264	0.001748252
BIOCARTA_NFKB_PATHWAY	21	1.91215931	0.001845018
PID_PI3KCI_PATHWAY	48	1.961340656	0.001865672
WP_SENESCENCE_AND_AUTOPHAGY_IN_CANCER	99	1.438630285	0.010544815
PID_P53_DOWNSTREAM_PATHWAY	125	1.35248466	0.026132404
MOOTHA_MITOCHONDRIA	400	1.259252988	0.028963415

https://doi.org/10.2147/JIR.S544597

Table 5 Gene Set Variation Analysis

Id	logFC	adj.P.Val
REACTOME_RHO_GTPASES_ACTIVATE_PAKS	−0.530450952	4.63E-13
PAPASPYRIDONOS_UNSTABLE_ATEROSCLEROTIC_PLAQUE_DN	−0.72754498	4.63E-13
GSE19198_CTRL_VS_IL21_TREATED_TCELL_6H_UP	0.402079877	3.45E-12
GO_BETA_2_MICROGLOBULIN_BINDING	0.791297562	7.05E-12
GO_DICHOTOMOUS_SUBDIVISION_OF_TERMINAL_UNITS_INVOLVED_IN_SALIVARY_GLAND_BRANCHING	0.799881156	7.05E-12
GO_REGULATION_OF_DENDRITIC_CELL_DIFFERENTIATION	0.659880403	7.05E-12
GO_COMPLEMENT_BINDING	0.502059467	7.78E-12
GO_POSITIVE_REGULATION_OF_CARDIAC_VASCULAR_SMOOTH_MUSCLE_CELL_DIFFERENTIATION	−1.03086206	7.78E-12
OCT1_03	−0.328112739	1.60E-11
GO_DICHOTOMOUS_SUBDIVISION_OF_AN_EPITHELIAL_TERMINAL_UNIT	0.655770191	1.69E-11

protein containing two C2 domains. TC2N has been reported to influence cancer cell behavior (higher expression is linked to worse prognosis in gastric cancer),[47] although its function in cardiovascular or immune contexts is not well characterized. Our identification of TC2N as a down-regulated hub gene in atherosclerosis is novel, raising the possibility that TC2N normally participates in vesicular trafficking or autophagic processes that restrain inflammatory activation – a hypothesis that warrants further investigation.SLC22A3 is an organic cation transporter involved in the transmembrane transport of various metabolites.[48] Genetic polymorphisms in SLC22A3 have been associated with altered risk of coronary heart disease,[49,50] type 2 diabetes,[51] and hypertension,[52] and this transporter may also affect blood lipid levels.[49] We observed that SLC22A3 expression was down-regulated in atherosclerotic lesions, aligning with the notion that reduced transporter activity could influence macrophage lipid handling and vascular inflammation in the plaque microenvironment.

Collectively, these five diagnostic markers appear to play pivotal roles in processes such as inflammation, immune cell function, and cell signaling. Given that atherosclerosis is fundamentally a chronic inflammatory disease, perturbations in these genes could have significant impacts on its initiation and progression. Indeed, the involvement of NEXN and SLC22A3 in atherosclerosis and coronary artery disease has been noted previously, which is congruent with our findings. Importantly, our study newly implicates MNDA, CD163L1 and TC2N in atherosclerosis, opening up new avenues to explore their utility as biomarkers or therapeutic targets in this disease context.

Beyond individual genes, we constructed a diagnostic nomogram based on the five hub genes to stratify atherosclerotic patients into high-risk and low-risk groups according to their gene expression profiles. As expected, the high-risk group (with overall higher risk scores from the five-gene model) exhibited enrichment of pro-atherogenic pathways. GSEA and GSVA revealed that pathways related to immune signaling and inflammation were up-regulated in the high-risk subgroup, including pathways such as B cell receptor signaling and TNF-α signaling, as well as biological processes like the positive regulation of vascular smooth muscle cell differentiation. These findings suggest that the identified gene signature captures a state of heightened immune activity and vascular remodeling, which are hallmarks of more advanced or active atherosclerotic disease.Furthermore, our network analysis of hub gene interactions provided additional context. The five hub genes were connected with numerous proteins, microRNAs (miRNAs), RNA-binding proteins (RBPs), and transcription factors known to regulate inflammation and apoptosis. For example, CTNNB1 (β-catenin), a key component of the Wnt signaling pathway, was identified as a protein potentially interacting with the hub genes. CTNNB1 can modulate cytokine and chemokine production and thereby influence immune cell activation and recruitment; indeed, certain CTNNB1 mutations reduce chemokine expression via miRNA-mediated mechanisms, leading to decreased immune cell infiltration in tumors.[53] Likewise, miR-146a-5p emerged as part of the hub gene regulatory network. This miRNA is an important negative feedback regulator of inflammation: it is up-regulated in response to inflammatory stimuli to help dampen excessive immune reactions.[54] In cardiovascular contexts, miR-146a-5p has been shown to protect cardiac cells by modulating matrix metalloproteinases and muscle contractility pathways after myocardial infarction,[55] and aberrant miR-146a-5p signaling is implicated in the progression of autoimmune diseases such as rheumatoid arthritis.[56] The presence of CTNNB1, miR-146a-5p, and other such molecules in the hub gene interaction

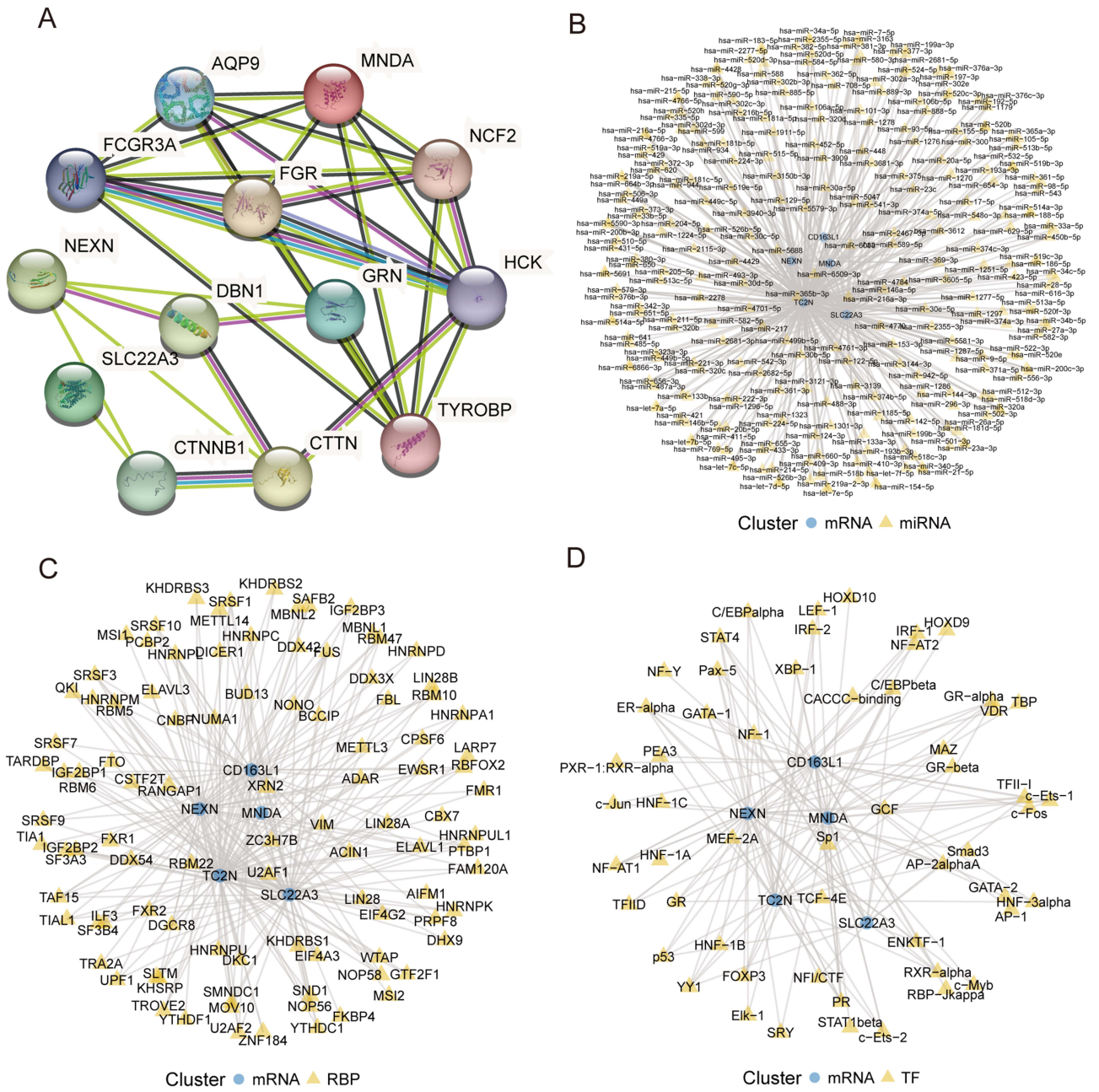

Figure 8 Construction of interaction networks involving hub genes. (**A**) Protein-Protein Interaction (PPI) network of hub genes, constructed using the STRING database. (**B**) mRNA-miRNA regulatory network, with blue circles denoting mRNA and yellow triangles indicating miRNA. (**C**) mRNA-RNA-Binding Protein (RBP) regulatory network, where blue circles symbolize mRNA and yellow triangles symbolize RBPs. (**D**) mRNA-Transcription Factor (TF) network, where blue circles signify mRNA and yellow triangles signify TFs. RNA-Binding Protein, RBP; Transcription Factor, TF.

networks suggests that our five key genes are integrated into broader immunometabolic regulatory circuits. This systems-level perspective reinforces the idea that MRGs do not act in isolation, but rather influence atherosclerosis as part of complex gene–network interactions that govern inflammation and cell survival.

We also characterized immune cell infiltration patterns in atherosclerotic samples and found them to be closely linked with the expression of the hub genes. Immune profiling by CIBERSORT and ssGSEA confirmed that atherosclerotic lesions have significantly higher infiltration of macrophages (particularly undifferentiated M0 macrophages) compared to control arterial tissues, consistent with the chronic inflammatory nature of the disease. Notably, this macrophage elevation was even more pronounced in the high-risk patient subgroup defined by our gene model, indicating that the

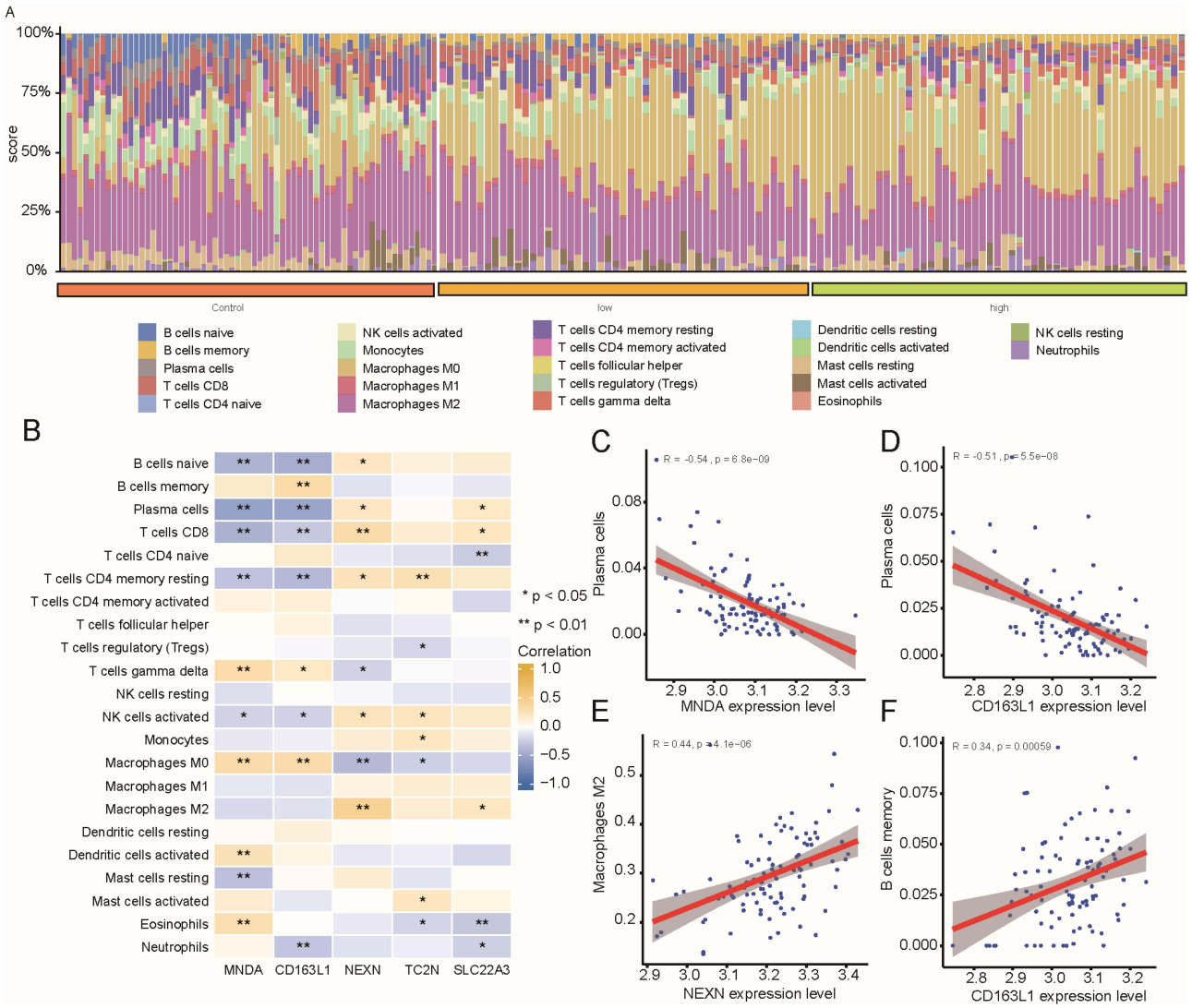

Figure 9 CIBERSORT immune analysis of atherosclerotic samples based on the combined dataset (**A**) Distribution of immune cells in Control, high-, and low-risk Atherosclerotic samples, as analyzed by CIBERSORT. (**B**) Heatmap illustrating the correlation between hub genes and varying levels of immune cell infiltration in Atherosclerotic samples, where blue denotes a negative correlation, and yellow denotes a positive correlation. (**C-F**) Scatter plots showing the correlation between specific genes and immune cell types: (**C**) Myeloid cell nuclear differentiation antigen (MNDA) and plasma cells, (**D**) CD163 molecule-like 1 (CD163L1) and plasma cells, (**E**) nexilin F-actin binding protein (NEXN) and M2 macrophages, and (**F**) CD163L1 and memory B cells.
Note: (*$P < 0.05$; **$P < 0.01$).

five-gene signature captures the extent of macrophage-driven inflammation. Correlation analyses further revealed that MNDA and CD163L1 expression levels were positively correlated with several immune cell types (including certain macrophage and lymphocyte populations), in line with their proposed pro-inflammatory roles. In contrast, NEXN, TC2N, and SLC22A3 levels were negatively correlated with immune cell abundance, consistent with the idea that lower expression of these genes accompanies a higher inflammatory state. Unsupervised clustering of the atherosclerotic samples further illustrated this immune imbalance. When samples were divided into two molecular subtypes, one subtype (Cluster B) was characterized by markedly higher MNDA and CD163L1 expression but lower TC2N and SLC22A3, and this subtype exhibited a greater accumulation of M0 macrophages and other immune cells. These results solidify the association between MRGs perturbations and immune cell dynamics in atherosclerosis. Our findings align with previous reports that mitophagy and immune activity are tightly interconnected.[7] In atherosclerotic plaques, macrophage-derived foam cells are pivotal drivers of disease progression,[57] and B cells and plasma cells can modulate autoimmune and inflammatory responses within lesions.[58] Mitophagy can influence these processes by removing

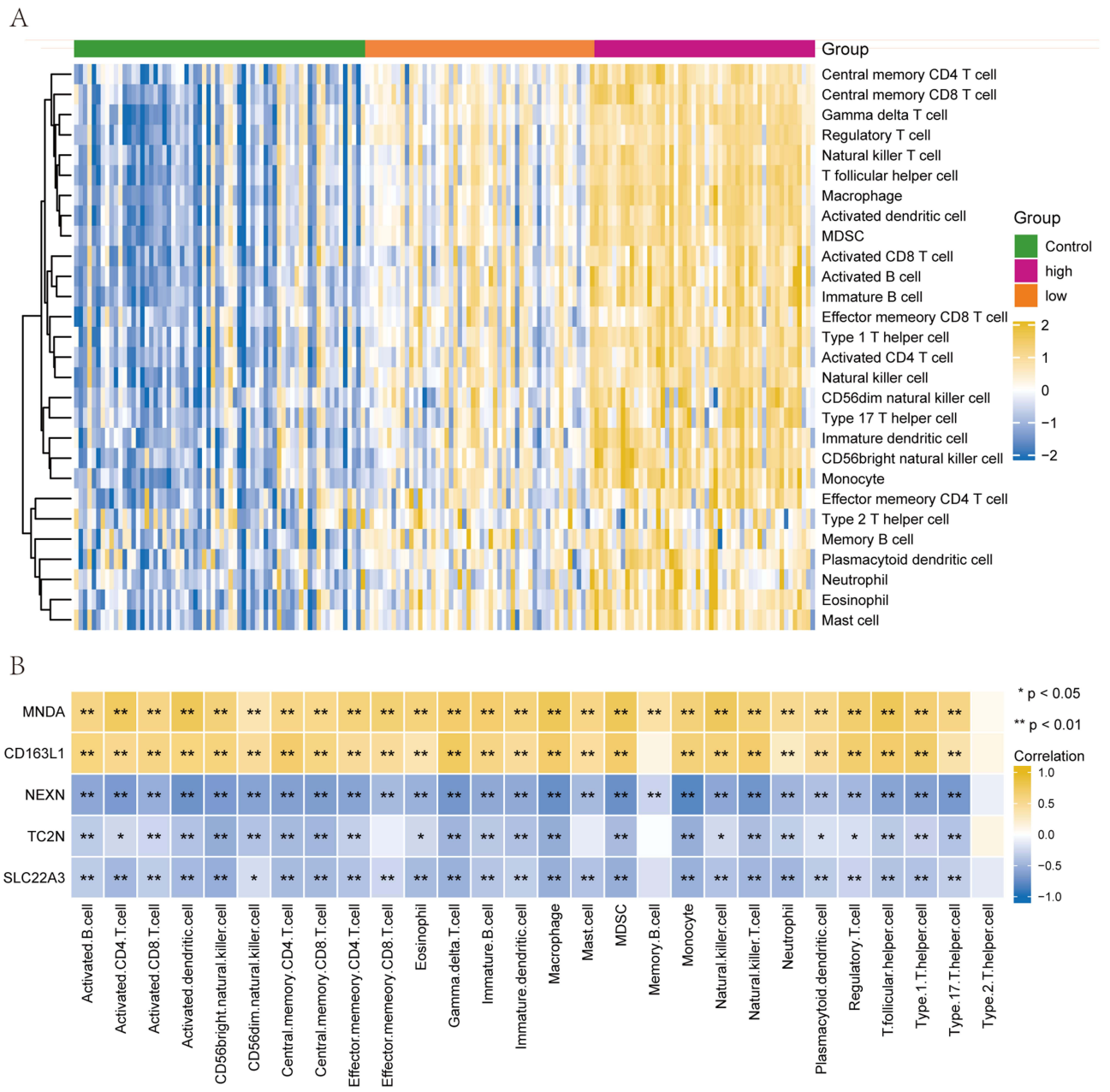

Figure 10 ssGSEA immune analysis of Atherosclerotic samples in the combined dataset. (**A**) Assessment of immune cell distribution in Control, high-, and low-risk Atherosclerotic samples using ssGSEA. (**B**) Heatmap illustrating the relationships between hub genes and various degrees of immune cell infiltration, as determined by ssGSEA.

Note: (*$P < 0.05$; **$P < 0.01$).

Abbreviations: Single-sample gene-set enrichment analysis, ssGSEA.

damaged mitochondria from immune cells, thereby preventing excessive inflammation (for instance, by limiting NLRP3 inflammasome activation). Indeed, enhanced mitophagy is known to promote macrophage polarization toward an anti-inflammatory M2 phenotype,[59] which helps stabilize plaques, and it may also affect T-cell activation and differentiation,[60] thus altering adaptive immune responses in the plaque microenvironment. Therefore, the shifts in immune cell populations associated with specific mitophagy gene changes in our study provide a mechanistic clue: insufficient mitophagy (as indicated by down-regulation of certain MRGs) could exacerbate immune cell-driven inflammation in atherosclerosis, whereas boosting mitophagy-related pathways might help re-establish immune homeostasis in diseased arteries.

https://doi.org/10.2147/JIR.S544597

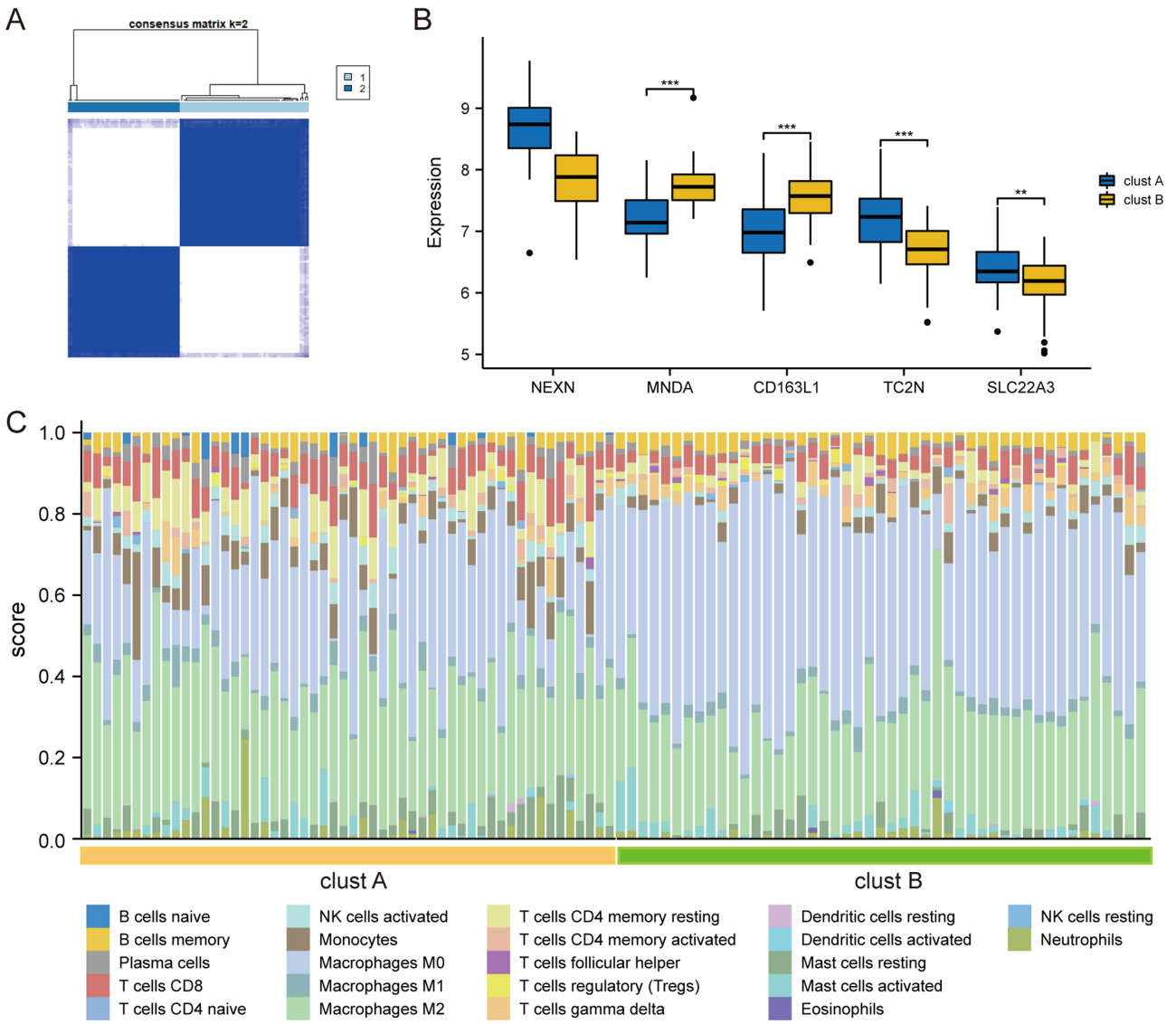

Figure 11 Unsupervised consensus clustering analysis of Atherosclerotic samples from the combined dataset (**A**) Distribution of sample clustering when segmented into two clusters. (**B**) Expression profiles of hub genes across atherosclerotic subtypes A and B, following division into two subtypes. (**C**) Status of immune cell infiltration in the two identified subtypes.
Note: (***P* < 0.01; ****P* < 0.001).

To further validate our computational findings, we performed in vitro experiments using macrophage models. Oxidized LDL (ox-LDL) stimulation was applied to mimic the pro-atherosclerotic, inflammatory environment in cultured cells.[32,33] In mouse RAW264.7 macrophages, ox-LDL exposure significantly up-regulated Mnda and Cd163l1 (the mouse homologs of MNDA and CD163L1), while Nexn, Tc2n, and Slc22a3 were down-regulated—changes fully consistent with the patterns observed in our human tissue analysis. Similarly, in phorbol ester-differentiated human THP-1 macrophages, MNDA transcript levels were markedly increased after ox-LDL treatment, and NEXN and SLC22A3 were decreased. (CD163L1 and TC2N in the THP-1 cells did not change significantly under ox-LDL, possibly reflecting differences between species or cell differentiation states). Despite these minor discrepancies, the overall concordance between our cell-based results and the bioinformatic predictions strengthens the validity of our findings. The observed up-regulation of MNDA and CD163L1 under inflammatory stress aligns with their roles in promoting macrophage activation and immune responses. Conversely, the down-regulation of NEXN, TC2N, and SLC22A3 in stimulated macrophages supports the idea that reduced expression of these genes accompanies the heightened

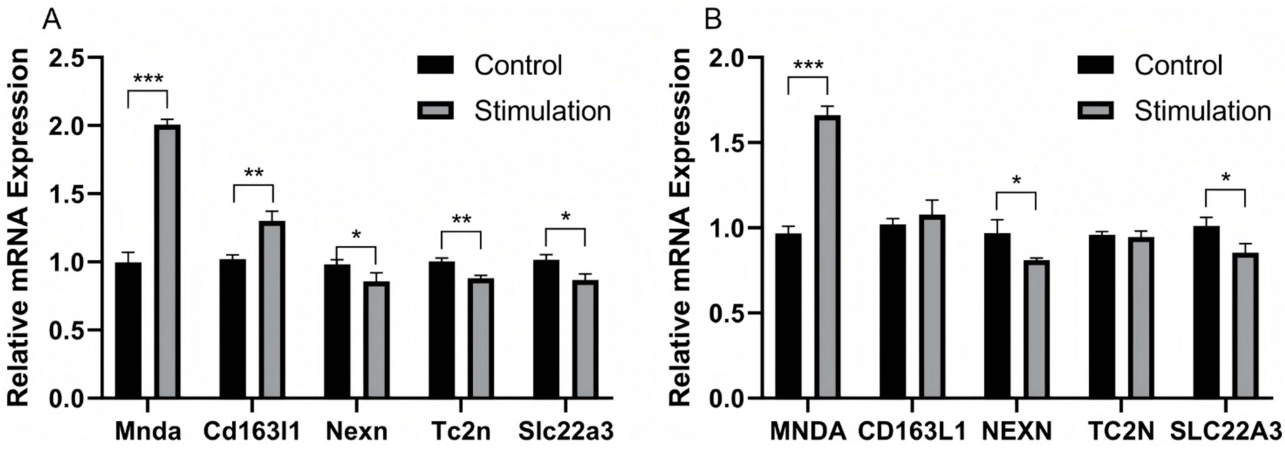

Figure 12 Validation of expression levels of selected mitophagy-related genes by qPCR (**A**) Relative mRNA expression of Mnda, Cd163l1, Nexn, Tc2n, and Slc22a3 in RAW264.7 cells treated with ox-LDL. β-actin was used as an internal control. (**B**) Relative mRNA expression of MNDA, CD163L1, NEXN, TC2N, and SLC22A3 in THP-1 cells treated with ox-LDL. GAPDH was used as an internal control. Data represent mean ± SD from three independent experiments. Statistical significance was determined by unpaired *t*-test.
Note: (*$P < 0.05$; **$P < 0.01$, ***$P < 0.001$).

inflammatory and metabolic activity characteristic of foam cell formation. By demonstrating that our hub genes respond to an atherogenic stimulus in two independent cell models (murine and human), these experiments suggest that the identified genes are not merely correlative markers but are actively involved in atherosclerosis-related cellular processes. However, we acknowledge that in vitro models are a simplification of the true disease environment, so further validation in vivo is needed.

This study has several limitations. First, our analyses relied on publicly available transcriptomic datasets which, despite careful batch correction and validation, may still contain intrinsic biases or offer limited clinical metadata. Because the data were retrospective, we could assess associations but not establish causation, and important clinical variables such as patient comorbidities or treatments could not be fully incorporated. Second, our experimental validation was limited to in vitro cell line models. Although ox-LDL-treated RAW264.7 and THP-1 macrophages helped substantiate the bioinformatic findings, these simplified systems cannot fully replicate the complexity of atherosclerotic lesions in vivo, which involve multiple cell types including endothelial cells and smooth muscle cells, intricate cell–cell interactions, and long-term processes such as plaque development and regression. These differences restrict the direct extrapolation of our results to clinical settings. Therefore, further in vivo investigations using animal models or patient samples will be essential to confirm the causative roles of the identified hub genes and to clarify their mechanistic connections to mitophagy and immunity in atherosclerosis. Despite these constraints, the study offers a valuable framework for elucidating the interplay between mitochondrial dysfunction and immune imbalance in atherosclerosis, and it provides a foundation for developing targeted diagnostic and therapeutic strategies.

Conclusions

In this study, we systematically investigated the relationship between mitophagy and immune infiltration in atherosclerosis and identified five hub genes—MNDA, CD163L1, NEXN, TC2N, and SLC22A3—as potential diagnostic biomarkers. These genes showed strong correlations with mitophagy-related pathways and immune cell infiltration profiles, indicating their potential roles in the interplay between mitochondrial homeostasis and immune dysregulation during atherogenesis. Experimental validation in ox-LDL–stimulated RAW264.7 and THP-1 macrophages confirmed expression patterns consistent with the bioinformatic predictions, strengthening the credibility of our integrative analysis. Overall, these findings provide new insights into the molecular links between mitophagy and immune imbalance in atherosclerosis and lay a foundation for future mechanistic research and the development of targeted diagnostic and therapeutic approaches.

Data Sharing Statement

All datasets analyzed in this study are publicly available. The raw data used in this investigation may be accessed via the public GEO database https://www.ncbi.nlm.nih.gov/geo/ (Accession numbers GSE43292 and GSE100927).

Ethics Statement

This study was conducted using publicly available human gene expression datasets (GSE43292 and GSE100927) from the GEO database, all of which had been previously approved by their respective institutional ethics committees with informed consent obtained from participants. According to the Measures for Ethical Review of Life Science and Medical Research Involving Human Subjects (issued February 18, 2023, China), Article 32, Items 1 and 2, research using publicly available human data that cannot be linked to identifiable individuals is exempt from review by the Institutional Review Board (IRB). Therefore, this study was exempt from additional ethical approval by the Ethics Committee of Peking University First Hospital.

Funding

This research was funded by High-Quality Clinical Research Project of Peking University First Hospital (2023HQ04) and by the PKU-Baidu Fund (2019BD019).

Disclosure

The authors declare that the research was conducted in the absence of any commercial or financial relationships that could be construed as a potential conflict of interest.

References

1. Popa-Fotea NM, Ferdoschi CE, Micheu MM. Molecular and cellular mechanisms of inflammation in atherosclerosis. *Front Cardiovasc Med*. 2023;10:1200341. doi:10.3389/fcvm.2023.1200341
2. Soehnlein O, Libby P. Targeting inflammation in atherosclerosis - from experimental insights to the clinic. *Nat Rev Drug Discov*. 2021;20(8):589–610. doi:10.1038/s41573-021-00198-1
3. Theofilis P, Oikonomou E, Tsioufis K, et al. The role of macrophages in atherosclerosis: pathophysiologic mechanisms and treatment considerations. *Int J Mol Sci*. 2023;24(11):9568. doi:10.3390/ijms24119568
4. Zhang Y, Weng J, Huan L, et al. Mitophagy in atherosclerosis: from mechanism to therapy. *Front Immunol*. 2023;14:1165507. doi:10.3389/fimmu.2023.1165507
5. Huynh DTN, Heo KS. Role of mitochondrial dynamics and mitophagy of vascular smooth muscle cell proliferation and migration in progression of atherosclerosis. *Arch Pharm Res*. 2021;44(12):1051–1061. doi:10.1007/s12272-021-01360-4
6. Wang L, Gao B, Wu M, et al. Profiles of immune cell infiltration in carotid artery atherosclerosis based on gene expression data. *Front Immunol*. 2021;12:599512. doi:10.3389/fimmu.2021.599512
7. Engelen SE, B RAJ, Zurke YX, et al. Therapeutic strategies targeting inflammation and immunity in atherosclerosis: how to proceed? *Nat Rev Cardiol*. 2022;19(8):522–542. doi:10.1038/s41569-021-00668-4
8. Zhao K, Wu Y, Zhao D, et al. Six mitophagy-related hub genes as peripheral blood biomarkers of Alzheimer's disease and their immune cell infiltration correlation. *Front Neurosci*. 2023;17:1125281. doi:10.3389/fnins.2023.1125281
9. Chen Y, Qin W, Li L, et al. Mitophagy: critical role in atherosclerosis progression. *DNA Cell Biol*. 2022;41(10):851–860. doi:10.1089/dna.2022.0249
10. Ayari H, Bricca G. Identification of two genes potentially associated in iron-heme homeostasis in human carotid plaque using microarray analysis. *J Biosci*. 2013;38(2):311–315. doi:10.1007/s12038-013-9310-2
11. Steenman M, Espitia O, Maurel B, et al. Identification of genomic differences among peripheral arterial beds in atherosclerotic and healthy arteries. *Sci Rep*. 2018;8(1):3940. doi:10.1038/s41598-018-22292-y
12. Davis S, Meltzer PS. GEOquery: a bridge between the Gene Expression Omnibus (GEO) and BioConductor. *Bioinformatics*. 2007;23(14):1846–1847. doi:10.1093/bioinformatics/btm254
13. Safran M, Solomon I, Shmueli O, et al. GeneCards 2002: towards a complete, object-oriented, human gene compendium. *Bioinformatics*. 2002;18(11):1542–1543. doi:10.1093/bioinformatics/18.11.1542
14. Muller C, Schillert A, Rothemeier C, et al. Removing batch effects from longitudinal gene expression - quantile normalization plus combat as best approach for microarray transcriptome data. *PLoS One*. 2016;11(6):e0156594. doi:10.1371/journal.pone.0156594
15. Ritchie ME, Phipson B, Wu D, et al. limma powers differential expression analyses for RNA-sequencing and microarray studies. *Nucleic Acids Res*. 2015;43(7):e47. doi:10.1093/nar/gkv007
16. Gene Ontology C. Gene Ontology Consortium: going forward. *Nucleic Acids Res*. 2015;43:D1049–56. doi:10.1093/nar/gku1179
17. Kanehisa M, Goto S. KEGG: kyoto encyclopedia of genes and genomes. *Nucleic Acids Res*. 2000;28(1):27–30. doi:10.1093/nar/28.1.27
18. Liao Y, Wang J, J JE, et al. WebGestalt 2019: gene set analysis toolkit with revamped UIs and APIs. *Nucleic Acids Res*. 2019;47(W1):W199–W205. doi:10.1093/nar/gkz401

19. L HM, Hung YH, Lee WM, et al. SVM-RFE based feature selection and Taguchi parameters optimization for multiclass SVM classifier [J]. *ScientificWorldJournal*. 2014;2014:795624. doi:10.1155/2014/795624
20. Rigatti SJ. Random Forest. *J Insur Med*. 2017;47(1):31–39. doi:10.17849/insm-47-01-31-39.1
21. Eng KH, Schiller E, Morrell K. On representing the prognostic value of continuous gene expression biomarkers with the restricted mean survival curve. *Oncotarget*. 2015;6(34):36308–36318. doi:10.18632/oncotarget.6121
22. Robin X, Turck N, Hainard A, et al. pROC: an open-source package for R and S+ to analyze and compare ROC curves. *BMC Bioinf*. 2011;12:77. doi:10.1186/1471-2105-12-77
23. Liberzon A, Birger C, Thorvaldsdottir H, et al. The Molecular Signatures Database (MSigDB) hallmark gene set collection. *Cell Syst*. 2015;1 (6):417–425. doi:10.1016/j.cels.2015.12.004
24. Yu G, Wang LG, Han Y, et al. clusterProfiler: an R package for comparing biological themes among gene clusters. *Omics*. 2012;16(5):284–287. doi:10.1089/omi.2011.0118
25. Hanzelmann S, Castelo R, Guinney J. GSVA: gene set variation analysis for microarray and RNA-seq data. *BMC Bioinf*. 2013;14:7. doi:10.1186/1471-2105-14-7
26. Szklarczyk D, Gable AL, Nastou KC, et al. The STRING database in 2021: customizable protein-protein networks, and functional characterization of user-uploaded gene/measurement sets. *Nucleic Acids Res*. 2021;49(D1):D605–D12. doi:10.1093/nar/gkaa1074
27. H LJ, Liu S, Zhou H, et al. starBase v2.0: decoding miRNA-ceRNA, miRNA-ncRNA and protein-RNA interaction networks from large-scale CLIP-Seq data. *Nucleic Acids Res*. 2014;42:D92–7. doi:10.1093/nar/gkt1248
28. Messeguer X, Escudero R, Farre D, et al. PROMO: detection of known transcription regulatory elements using species-tailored searches. *Bioinformatics*. 2002;18(2):333–334. doi:10.1093/bioinformatics/18.2.333
29. Chen B, Khodadoust MS, L LC, et al. Profiling Tumor Infiltrating Immune Cells with CIBERSORT. *Methods Mol Biol*. 2018;1711:243–259. doi:10.1007/978-1-4939-7493-1_12
30. Xiao B, Liu L, Li A, et al. Identification and verification of immune-related gene prognostic signature based on ssGSEA for osteosarcoma. *Front Oncol*. 2020;10:607622. doi:10.3389/fonc.2020.607622
31. Wilkerson MD, Hayes DN. ConsensusClusterPlus: a class discovery tool with confidence assessments and item tracking. *Bioinformatics*. 2010;26 (12):1572–1573. doi:10.1093/bioinformatics/btq170
32. Zhao Q, Zhong Y, Li Z, et al. Anti atherosclerosis effect and mechanism of a novel curcumin analogue CACN136: regulating macrophage M1/M2 polarization and lipid metabolism. *Front Pharmacol*. 2025;16:1632647. doi:10.3389/fphar.2025.1632647
33. Moon HR, Yun JM. Protective effect of Allium hookeri water extract and its main compound, Cycloalliin, on foam cell formation in THP-1-derived macrophages. *Food Nutr Res*. 2025;69. doi:10.29219/fnr.v69.10763
34. Mao Q, Luo B, Mei J, et al. Macrophage Dicer promotes tolerogenic apoptotic cell clearance and immune tolerance by inhibiting pentose phosphate pathway activity. *Cell Mol Immunol*. 2021;18(7):1841–1843. doi:10.1038/s41423-021-00693-w
35. Baeyens N. Fluid shear stress sensing in vascular homeostasis and remodeling: towards the development of innovative pharmacological approaches to treat vascular dysfunction. *Biochem Pharmacol*. 2018;158:185–191. doi:10.1016/j.bcp.2018.10.023
36. L MP, Obendorf L, Jatzlau J, et al. Atheroprone fluid shear stress-regulated ALK1-Endoglin-SMAD signaling originates from early endosomes [J]. *BMC Biol*. 2022;20(1):210. doi:10.1186/s12915-022-01396-y
37. Johnson RC, Kim J, Natkunam Y, et al. Myeloid Cell Nuclear Differentiation Antigen (MNDA) expression distinguishes extramedullary presentations of myeloid leukemia from blastic plasmacytoid dendritic cell neoplasm. *Am J Surg Pathol*. 2016;40(4):502–509. doi:10.1097/PAS.0000000000000595
38. Bottardi S, Guieze R, Bourgoin V, et al. MNDA controls the expression of MCL-1 and BCL-2 in chronic lymphocytic leukemia cells. *Exp Hematol*. 2020;88:68–82e5. doi:10.1016/j.exphem.2020.07.004
39. Gu L, Casserly D, Brady G, et al. Myeloid cell nuclear differentiation antigen controls the pathogen-stimulated type I interferon cascade in human monocytes by transcriptional regulation of IRF7. *Nat Commun*. 2022;13(1):14. doi:10.1038/s41467-021-27701-x
40. Van Beers J, Schwarte CM, Stammen-Vogelzangs J, et al. The rheumatoid arthritis synovial fluid citrullinome reveals novel citrullinated epitopes in apolipoprotein E, myeloid nuclear differentiation antigen, and beta-actin. *Arthritis Rheum*. 2013;65(1):69–80. doi:10.1002/art.37720
41. González-Domínguez É, Samaniego R, L F-SJ, et al. CD163L1 and CLEC5A discriminate subsets of human resident and inflammatory macrophages in vivo. *J Leukoc Biol*. 2015;98(4):453–466. doi:10.1189/jlb.3HI1114-531R
42. Semnani-Azad Z, Blanco Mejia S, Connelly PW, et al. The association of soluble CD163, a novel biomarker of macrophage activation, with type 2 diabetes mellitus and its underlying physiological disorders: a systematic review. *Obes Rev*. 2021;22(9):e13257. doi:10.1111/obr.13257
43. Yamashita M, Utsumi Y, Nagashima H, et al. S100A9/CD163 expression profiles in classical monocytes as biomarkers to discriminate idiopathic pulmonary fibrosis from idiopathic nonspecific interstitial pneumonia. *Sci Rep*. 2021;11(1):12135. doi:10.1038/s41598-021-91407-9
44. Yamaguchi Y, Gibson J, Ou K, et al. PD-L1 blockade restores CAR T cell activity through IFN-γ-regulation of CD163+ M2 macrophages. *J Immunother Cancer*. 2022;10(6):e004400. doi:10.1136/jitc-2021-004400
45. Yang Q, M BA, Ezekian JE, et al. Determining the likelihood of disease pathogenicity among incidentally identified genetic variants in rare dilated cardiomyopathy-associated genes. *J Am Heart Assoc*. 2022;11(19):e025257. doi:10.1161/JAHA.122.025257
46. Hu YW, Guo FX, Xu YJ, et al. Long noncoding RNA NEXN-AS1 mitigates atherosclerosis by regulating the actin-binding protein NEXN. *J Clin Invest*. 2019;129(3):1115–1128. doi:10.1172/JCI98230
47. Xu J, Ou X, Li J, et al. Overexpression of TC2N is associated with poor prognosis in gastric cancer. *J Cancer*. 2021;12(3):807–817. doi:10.7150/jca.50653
48. Chen L, Hong C, Chen EC, et al. Genetic and epigenetic regulation of the organic cation transporter 3, SLC22A3. *Pharmacogenomics J*. 2013;13 (2):110–120. doi:10.1038/tpj.2011.60
49. Zheng PF, Yin RX, Cao XL, et al. Effect of SYTL3-SLC22A3 Variants, Their Haplotypes, and G x E interactions on serum lipid levels and the risk of coronary artery disease and ischaemic stroke. *Front Cardiovasc Med*. 2021;8:713068. doi:10.3389/fcvm.2021.713068
50. Li L, He M, Zhou L, et al. A solute carrier family 22 member 3 variant rs3088442 G-->A associated with coronary heart disease inhibits lipopolysaccharide-induced inflammatory response. *J Biol Chem*. 2015;290(9):5328–5340. doi:10.1074/jbc.M114.584953
51. Li Z, Yuan X, Liu X, et al. The Influence of SLC22A3 genetic polymorphisms on susceptibility to type 2 diabetes mellitus in chinese population. *Diabetes Metab Syndr Obes*. 2023;16:1775–1781. doi:10.2147/DMSO.S412857

52. Sallinen R, Kaunisto MA, Forsblom C, et al. Association of the SLC22A1, SLC22A2, and SLC22A3 genes encoding organic cation transporters with diabetic nephropathy and hypertension. *Ann Med*. 2010;42(4):296–304. doi:10.3109/07853891003777109
53. Xiao X, Mo H, Tu K. CTNNB1 mutation suppresses infiltration of immune cells in hepatocellular carcinoma through miRNA-mediated regulation of chemokine expression. *Int Immunopharmacol*. 2020;89:107043. doi:10.1016/j.intimp.2020.107043
54. Iacona JR, Lutz CS. miR-146a-5p: expression, regulation, and functions in cancer. *Wiley Interdiscip Rev RNA*. 2019;10(4):e1533. doi:10.1002/wrna.1533
55. Dong M, Chen D, Zhu Y, et al. Impaired regulation of MMP2/16-MLCK3 by miR-146a-5p increased susceptibility to myocardial ischaemic injury in aging mice. *Cardiovasc Res*. 2023;119(3):786–801. doi:10.1093/cvr/cvac104
56. Chen X, Xie L, Jiang Y, et al. LCK, FOXC1 and hsa-miR-146a-5p as potential immune effector molecules associated with rheumatoid arthritis. *Biomarkers*. 2023;28(1):130–138. doi:10.1080/1354750X.2022.2150315
57. Kloc M, Kubiak JZ, Ghobrial RM. Macrophage-, dendritic-, smooth muscle-, endothelium-, and stem cells-derived foam cells in atherosclerosis. *Int J Mol Sci*. 2022;23(22):14154. doi:10.3390/ijms232214154
58. Kao D, Lux A, Schwab I, et al. Targeting B cells and autoantibodies in the therapy of autoimmune diseases. *Semin Immunopathol*. 2014;36(3):289–299. doi:10.1007/s00281-014-0427-7
59. H WJ, Li DY, Liang S, et al. Macrophage autophagy in macrophage polarization, chronic inflammation and organ fibrosis. *Front Immunol*. 2022;13:946832. doi:10.3389/fimmu.2022.946832
60. Dowling SD, Macian F. Autophagy and T cell metabolism. *Cancer Lett*. 2018;419:20–26. doi:10.1016/j.canlet.2018.01.033